Scilight

Urban and Building Science

https://www.sciltp.com/journals/ubs

Article

Mitigation of Airborne Disease Transmission and Particle Capture by Ceiling Fan Ventilation in Street Stores

Xiaofei Han [1,†], Mingyuan Qin [2,3,†], Jiayu Li [4], Haoxiang Zhan [1,5,*], Xiaolei Yuan [6] and Norhayati Mahyuddin [1,*]

[1] Centre for Building, Construction & Tropical Architecture, Faculty of Built Environment, Universiti Malaya, Kuala Lumpur 50603, Malaysia
[2] School of Architecture and Civil Engineering, Xihua University, Chengdu 610039, China
[3] Department of Mechanical Engineering, Universiti Malaya, Kuala Lumpur 50603, Malaysia
[4] Center for the Built Environment, University of California, Berkeley, CA 94720, USA
[5] Tsinghua Shenzhen International Graduate School, Tsinghua University, Shenzhen 518055, China
[6] Department of Mechanical Engineering, Aalto University, FI-00076 Espoo, Finland
* Correspondence: haoxiang.zhan@sz.tsinghua.edu.cn (H.Z.); hayati@um.edu.my (N.M.)
† These authors contributed equally to this work.

How To Cite: Han, X.; Qin, M.; Li, J.; et al. Mitigation of Airborne Disease Transmission and Particle Capture by Ceiling Fan Ventilation in Street Stores. *Urban and Building Science* **2026**, *2*(2), 1. https://doi.org/10.53941/ubs.2026.100007

Received: 26 September 2025
Revised: 22 January 2026
Accepted: 2 February 2026
Published: 3 February 2026

Abstract: Street stores are high-density environments that are regarded as high-risk public spaces during epidemics and influenza outbreaks. The use of ceiling fans (CF) to improve airflow organization is considered an effective strategy for mitigating airborne virus transmission. While CFs offer advantages such as energy efficiency, cost-effectiveness, and ease of implementation, their effectiveness has not been quantitatively described. In this study, tracer gas diffusion experiments combined with computational fluid dynamics (CFD) simulations were conducted to evaluate various CF operation strategies in a representative street store in northern China. Occupant infection risk was further quantified using the Wells-Riley model. Results indicated that in enclosed environments, CFs could provide only short-term reductions in breathing-zone concentrations. When combined with natural ventilation (NV), particle removal efficiency increased by at least 60%. Comparative analysis revealed that low CF speeds were insufficient for particle removal, while excessively high speeds facilitated viral dispersion. Optimal control of overall infection risk was achieved when NV+CF operated at 196 RPM.

Keywords: airflow patterns; ceiling fan; CFD; ventilation strategy

1. Introduction

Airborne diseases pose a significant public health threat, particularly within enclosed indoor spaces [1,2]. Studies have consistently demonstrated that poorly ventilated indoor environments significantly increase the risk of airborne pathogen transmission as a result of viral particle accumulation [3]. Small-scale commercial spaces, such as street stores, exhibit distinctive virus transmission dynamics. This is largely due to frequent but short-duration customer visits and unpredictable occupancy patterns. Limited ventilation infrastructure further exacerbates the problem, especially when compared with larger buildings such as restaurants [4,5], offices [6], mosques [7], and schools [8]. Despite their prevalence, the specific roles played by these street stores in airborne infection transmission, as well as optimal ventilation solutions tailored to such environments, remain insufficiently studied.

Ventilation strategies, particularly airflow management, have been shown to be critical in mitigating airborne transmission through the effective removal and/or dilution of virus-laden aerosols [9–12]. Ceiling fans (CFs) have emerged as a practical and cost-effective ventilation solution, commonly employed to enhance indoor air circulation in street stores [13]. Prior studies indicate that CFs can influence viral transmission by modifying

airflow patterns, accelerating particle deposition, diluting airborne pathogens, and potentially generating localized negative-pressure zones [14]. However, the effectiveness of ceiling fans in reducing virus concentrations and controlling airborne infection risks within street stores remains inadequately assessed. Critical knowledge gaps remain regarding the optimal operational parameters for CFs, including rotation speed, rotation direction, and the integration of mechanical with natural ventilation strategies [15].

Given their low cost, CFs are widely used to enhance indoor air movement and can help reduce airborne infection risk [16]. Existing studies typically rely on either measurements [17] or simulations [18], including approaches that record indoor air speed, airflow direction, and pollutant concentration. Measurements provide direct observations of real environments and capture factors that are difficult to model; however, transient behavior is challenging to resolve, and experiments usually provide concentration time series only at discrete sampling points. Because detailed measurements are time-consuming and costly, many researchers therefore use CFD to examine velocity, temperature, and concentration fields and to visualize particle transport across a wider range of operating scenarios. Both approaches highlight the central role of indoor air movement in airborne transmission. Accordingly, this study adopts a hybrid approach that combines tracer-gas diffusion experiments with CFD simulations

Particular attention is given to identifying optimal CF strategies tailored to street stores by systematically investigating key factors, including CF rotation direction (i.e., downward or upward airflow), rotation speed, and the interplay between fan-induced and natural ventilation conditions [19–22]. The present work aims to elucidate effective, practical, and scalable CF strategies capable of significantly reducing airborne infection risks within small-scale commercial indoor settings.

2. Materials and Methods

2.1. Experimental Sites

The street stores considered in this study are small commercial units of a standardized design in China, located beneath residential buildings and facing the street. As shown in Figure 1, a real estate agency was selected as the representative site for the experiments, where air exchange rate and tracer gas diffusion experiments were conducted. Figure 1a,b show photographs of the site; the main entrance faces north. A physical model of the store is shown in Figure 1c. The room measures 3400 mm × 4800 mm × 3200 mm and includes a cash register near the entrance. The table measures 1700 mm in size and features a stepped tabletop design, with an outer height of 900 mm and an inner height of 700 mm. The main entrance, which can be opened to a size of 1000 mm, is shown in the image, while in reality, there is also a 500 mm window that cannot be opened, as indicated in the real-life photo. The experimental period of this study spanned from 10 May to 16 May 2024. The store remained closed during this period. Its original ventilation strategy relied on natural ventilation, with the main entrance functioning as the primary opening for airflow. To represent the most common layout of these standardized stores, the CFD model was simplified to include only the fundamental architectural envelope and the essential employee desk, while other non-standard furnishings were omitted. For the simulation, the contaminant release point and the standing position of the occupant were set directly beneath the ceiling fan to analyze the most representative airflow and exposure scenario.

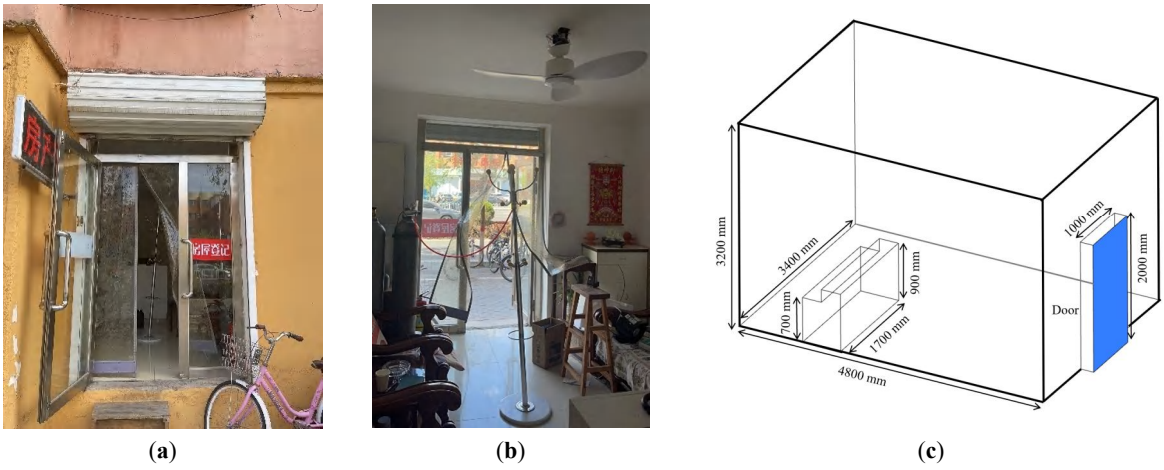

(**a**) (**b**) (**c**)

Figure 1. Real-estate agency store: (**a**) Store photo (outdoor); (**b**) Store photo (indoor); (**c**) Building physical model.

2.2. Ceiling Fan

For this study, a household CF with a diameter of 107 cm and three blades (Figure 2a) was selected as the experimental apparatus. The CF was controlled via a remote control, allowing adjustments of both speed and rotation direction, as illustrated in Figure 2b. It was installed at a height of 2700 mm above the floor and positioned near the center of the ceiling in the experimental site (Figure 2c).

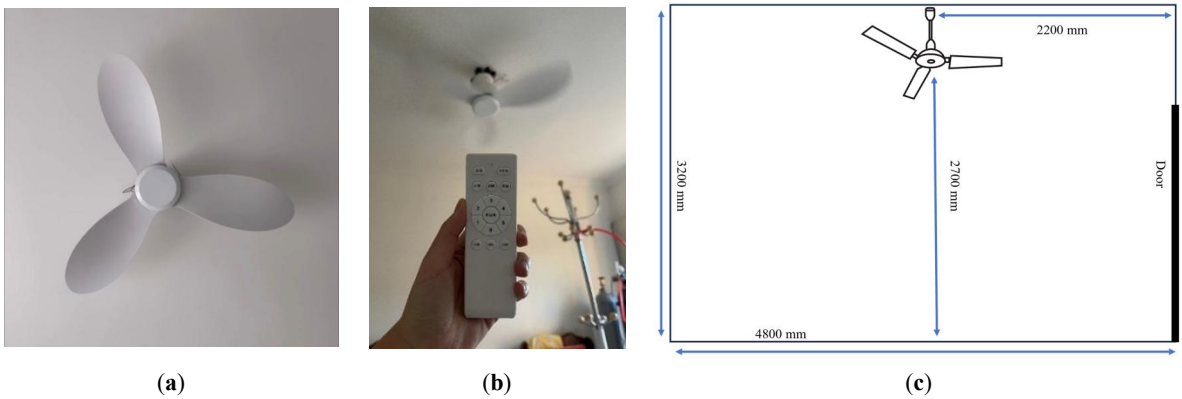

(**a**) (**b**) (**c**)

Figure 2. (**a**) Ceiling fan; (**b**) Controller; (**c**) Ceiling fan installation location.

Table 1 summarizes the detailed parameters of the CF used in this study. These parameters include both upward and downward rotation modes. Fan speed (RPM) was a critical parameter, with values of 0, 120, 196, and 252 RPM corresponding to settings 0, CF-1, CF-3, and CF-6, respectively.

Table 1. Ceiling fan parameters.

Item	Parameter
Height	38 cm
Diameter	107 cm
Number of blades	3
Material of blade	ABS
Blade Size	550 mm × 200 mm
Blade Angle	14°
Downward rotating gears	0–6
Upward rotating gears	0–6
RPM	1st gear: 120 RPM 3rd gear: 196 RPM 6th gear: 252 RPM

2.3. Tracer Gas Diffusion Experiment

To investigate contaminant dispersion in a street store and the effect of different fan-assisted ventilation strategies, tracer-gas diffusion experiments were conducted. CO_2 has been widely used as a tracer because it is easy to detect and cost-effective, enabling multipoint indoor measurements [23]. Accordingly, CO_2 was used as the tracer gas in this study.

2.3.1. Experimental Procedure

Throughout the experiment, the store door served as both the air inlet and outlet. As illustrated in Figure 3, to evaluate the vertical airflow distribution generated by the ceiling fan, four measurement points (A, B, C, D) were set at heights of 175 cm, 110 cm, and 50 cm above the floor. These heights correspond to the breathing zones of a standing adult (~160 cm), a seated person (~110 cm), and a young child (~50 cm), respectively. Point A is located directly under the fan to assess the direct airflow from the blades. Point B is placed in the corner near the doorway to examine airflow diffusion to typically stagnant areas. Point C is positioned in the corner farthest from the door to verify airflow coverage in the deepest part of the room. Point D is situated at the doorway to evaluate air exchange efficiency. During the experiment, the initial CO_2 concentration at each measurement point was recorded. A CO_2 concentration range of 500–650 ppm was maintained as the baseline for the unoccupied condition of the room. The CO_2 release rate was set at 0.5 L/min, corresponding to the average respiratory emission of an occupant.

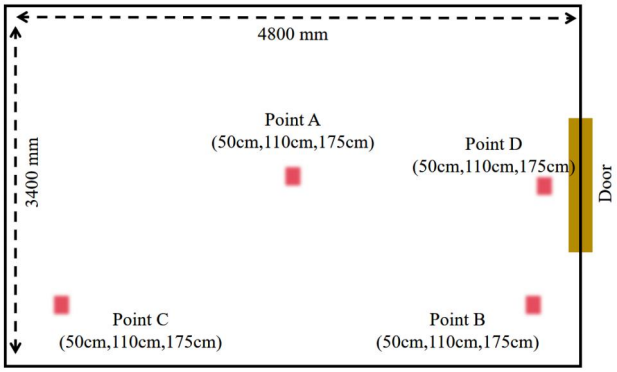

Figure 3. Experimental Measurement Locations.

The procedure for all experiments generally followed the framework illustrated in Figure 4. Each experimental run lasted 30 min and consisted of four main phases. Phase A: Preparation. The room was ventilated until the CO_2 concentration returned to the baseline range, and initial parameters (CO_2 concentration, temperature, humidity, and wind speed) were measured before releasing CO_2. Phase B: Ventilation configuration. Various ventilation strategies, including the fan and natural ventilation (NV), were activated to stabilize the airflow, which was maintained for 3 min to minimize interference. Phase C: Tracer experiment. After stabilization, CO_2 was released as a tracer for 10 min, and its concentration at each measurement point was recorded at 20-s intervals. Phase D: Post-processing. This phase assessed the continued effect of fan ventilation on residual virus-laden particles after CO_2 release ceased. Data collection continued until the room returned to its initial conditions, after which all instruments and equipment were powered down, marking the completion of the experiment. However, the biological decay of the virus was not considered for this study, as the entire study duration was less than 30 min. Given that the estimated lifespan of SARS-CoV-2 is approximately 1.1 h, the virus would remain viable during the short exposure time used in this experiment [24].

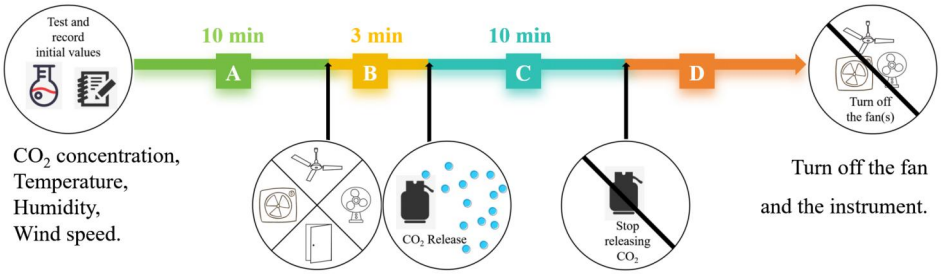

Figure 4. Experimental procedure.

2.3.2. Experimental Equipment

The instrumentation consisted of gas release devices, gas detection instruments, and environmental monitoring equipment. The CO_2 release system (Figure 5a) comprised two 40 L cylinders of liquefied CO_2 with a combined weight of 90 kg. Pressure gauges and flow meters were installed at the outlet of the cylinders (Figures 5b,c) to allow precise control of the CO_2 release during the experiments. A QingPing air detector (Figure 5d) was used to measure CO_2 concentration, temperature, and other parameters [25]. Indoor air velocity was measured using a Testo405i thermal anemometer (Figure 5e), with a test range of 0–30 m/s and an accuracy of ± (0.1 m/s + 5%) [26]. The detailed specifications of all instruments are provided in Table 2.

Table 2. Experimental instrumentation.

Device Names	Type	Range	Allowed Error
Qingping air detector	T_{in}	−10–50 °C	±0.8 °C
Refined	RH	0–100%	±8%
	CO_2	0–9999 ppm	±15%
	Total volatile organic compounds (TVOC)	0.005–9.999 mg/m^3	±20%
	$PM_{2.5}$	0–999 μg/m^3	±10 μg/m^3
Pressure gauge	CO_2	0–25 MPa	–
Flow meter	CO_2	0–25 L/min	–
Carbon dioxide cylinder	CO_2	40 L	–

(**a**) (**b**) (**c**) (**d**) (**e**)

Figure 5. Experimental instrumentation: (**a**) Carbon dioxide cylinder (CO_2 release system), (**b**) Pressure gauge, (**c**) Flow meter, (**d**) Qingping air detector (Reprinted with permission from Ref. [25]. 2026, Xiaofei Han), (**e**) Testo405i thermal anemometer (Reprinted with permission from Ref. [26]. 2026, Xiaofei Han).

2.4. CFD Simulation

Tracer gas experiments alone cannot fully compare fan operating scenarios or capture complete virus transmission pathways. CFD simulations address these gaps by visualizing particle dispersion, extending beyond measured locations, and highlighting areas of elevated infection risk within the street store.

2.4.1. Geometry

A CFD physical model of the street store is shown in Figure 6. The model was developed in ANSYS Workbench 2022 R2. The emitter was positioned 2 m from the doorway, near the room center and directly beneath the ceiling fan, facing the employee table. The emitter was represented as a 1750 mm-high simplified rectangular body to reduce computational cost and mesh count without materially affecting the airflow predictions, consistent with prior studies [27]. A 10 × 30 mm^2 rectangular inlet at the mouth was defined for particle injection.

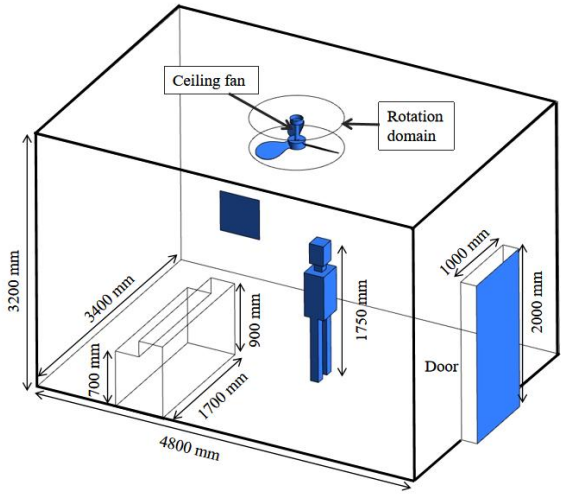

Figure 6. Physical models of street stores.

2.4.2. Mathematical Model

The RNG k-ε turbulence model can effectively simulate indoor airflow and the particles dispersion. For incompressible turbulent flows, the RNG formulation provides transport equations for mass and momentum with good accuracy at reasonable computational cost [28].

The simulations in this paper assume that the fluid phase in the store is incompressible, and the continuous and momentum equations of the flow field can be expressed as Equations (1) and (2), respectively:

$$\frac{\partial u_i}{\partial x_i} = 0 \quad (1)$$

$$\rho \frac{\partial u_i}{\partial t} + \rho u_j \frac{\partial u_i}{\partial t} = -\frac{\partial P}{\partial x_i} + \frac{\partial}{\partial x_j}\left(\mu \frac{\partial u_i}{\partial u_j} - \rho \overline{u_i' u_j'}\right) \quad (2)$$

where u_i and u_j are the mean values of the velocity component $(i, j = 1,2,3)$, μ is the fluid viscosity coefficient, P and ρ are the mean values of the pressure and fluid density, respectively, and $\rho \overline{u_i' u_j'}$ is the Reynolds stress term.

Using a Lagrange approach, DPM [29–31], which relates to the processes of aerosol particle dispersion throughout the required computational domain, is calculated as a sequence of differential equations.

$$\frac{dx_p}{dt} = u_p \quad (3)$$

For the motion of isothermal particles, the following ordinary differential equation is solved because of the balance between inertial forces and external forces applied to the particle.

$$m_p = \frac{du_p}{dt} = \Sigma F \quad (4)$$

where x_p is the particle position vector, u_p is the speed of particles, m_p is the particle mass, and ΣF is the force acting on particles.

2.4.3. Meshing and Grid Independence Check

To solve the governing equations, the computational domain is discretized using the finite volume method [32], and the resulting mesh is shown in Figure 7. The domain was primarily meshed with tetrahedral elements. In total, approximately 5.51 million cells were used, with local refinement around the human model and the CF.

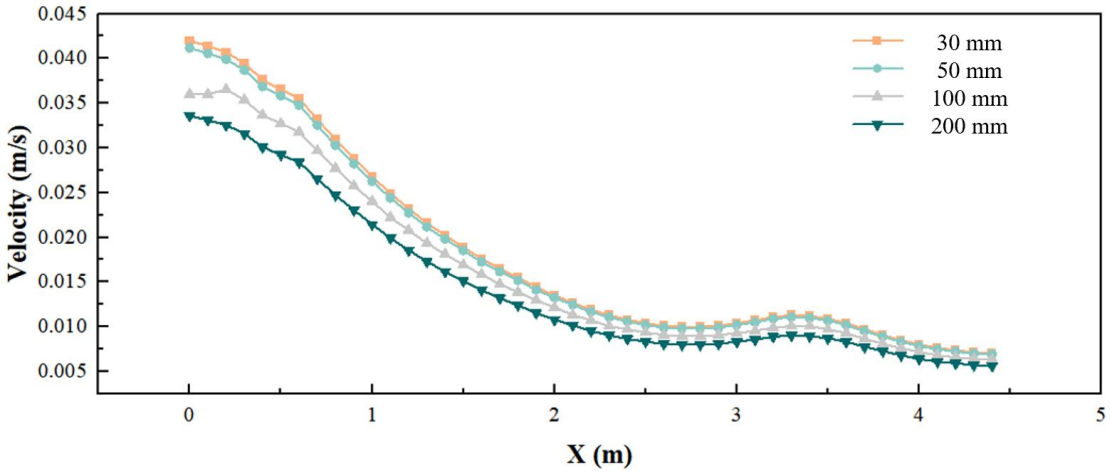

Figure 7. Mesh schematic of 20–50 mm.

As the computational cost increases with increasing the cell number, a mesh sensitivity study was conducted in order to get a reliable solution using as few cells as possible. To ensure that the results are grid independent, a total of four grid sizes (30, 50, 100 and 200 mm) were created for independence testing, as shown in Table 3. Grid volumes of 0.9 million, 1.5 million, 5.5 million, and 7.5 million were assumed, respectively. The solution showed good convergence across these meshes, and refining the grid from 50 to 30 mm did not materially change the flow field (average difference < 10%). Therefore, the 50 mm mesh was selected to balance accuracy and computational efficiency.

Table 3. Independence test grid generation information.

Mesh	Minimum Grid Size (mm)	Total Number of Grids
More refined	30	7,558,615
Refined	50	5,515,117
Medium	100	1,553,971
Coarse	200	998,115

To reduce computational cost, the outer mesh of the rotating frame of reference employed hexahedral elements. The rotating frame of reference comprised 28% of the total mesh to capture the aerodynamics around

the CF. The mesh was optimized in Gambit to achieve a skewness below 0.86. The numerical solution was obtained using a second-order discretization under isothermal indoor conditions (no heat sources).

2.4.4. Boundary Condition

During the simulations, the fan boundary conditions were tuned so that the simulated wind speeds were consistent with the measured values. Table 4 summarize the key model settings [17]. Given the negligible influence of gravity on 3 μm aerosol particles, gravitational settling was neglected [33]. Three particle–boundary interaction types were specified based on surface characteristics and expected particle behavior: Trap: (floor, furniture, and other interior surfaces), where particles were assumed to be captured upon contact and their trajectories terminated; Reflection (ceiling and vertical walls), where particles were assumed to reflect elastically and continue dispersing (a conservative assumption that may slightly overestimate particle residence time); and Escape (the mouth of the human model and the room outlets), representing the exhalation source and ventilation removal, respectively.

Table 4. Details of the DPM for liquid particles.

Particle Component	Virus Particles
Density	1000 kg/m^3
Specific heat capacity	5.854 kJ/kg·K
Drag law	Stokes-Cunningham
Turbulent dispersion	Discrete random walk model
Injection	Particle size: 3 μm Particle type: Inert Injection velocity: 0.5 m/s Injection type: surface Injection angle: normal

In addition, to simulate the airflow field, it was assumed that in the store, the variables were stable. The CFD simulation was run until residuals became constant, with more than 10,000 iterations in all cases. The calculations are considered to have converged when the non-dimensional residuals, velocity components, energy, k, and ε of the continuity equation are all less than 10^{-6} and when the surface specific monitoring variables are stable. In this paper, the energy balance and mass balance are also examined to help determine convergence. An initial time step of minimum 0.01 s and a total time of 300−600 s were used to track the spatio-temporal transport properties of the released particles during the release period.

2.5. Case Setting

Building on previous studies, the influence of CF speed was examined. As shown in Table 5, Cases 1–3 represent increasing ceiling fan speeds with the fan operating alone. A comparison with Case 4–5 highlights the differences between scenarios with and without NV.

Table 5. Experimental cases for ceiling fans.

Case	Ceiling Fan	Natural Ventilation
Case 1	CF-1	OFF
Case 2	CF-3	OFF
Case 3	CF-6	OFF
Case 4	CF-3	ON
Case 5	CF-6	ON

Since many scenarios could not be achieved in the actual tests, Cases 6–12 were designed for the study of CFs, as shown in Table 6. Similar to the actual measurements, these cases were used to verify the accuracy of the simulation. In contrast, they were also applied to explore additional influencing factors. During the simulation validation, the number of particles captured on all room surfaces was quantified, providing a clearer characterization of the propagation process. In addition, in the time analysis, the simulations were defined for two sequential customers: guest 1 and guest 2.

Table 6. Simulation cases for ceiling fans.

Case	Ceiling Fan	Natural Ventilation
Case 6	CF-1	OFF
Case 7	CF-3	OFF
Case 8	CF-6	OFF
Case 9	CF-3	ON
Case 10	UCF *-3	OFF
Case 11	UCF-6	OFF
Case 12	UCF-3	ON

* UCF: upward rotating ceiling fan.

3. Results

3.1. Airflow Patterns and Validation

Based on the velocity streamline diagram (Figure 8) of the downward-rotating CF in a street-store configuration, the induced airflow can be clearly divided into three characteristic zones: a high-velocity jet core zone, a recirculation zone, and a transitional entrainment zone between them.

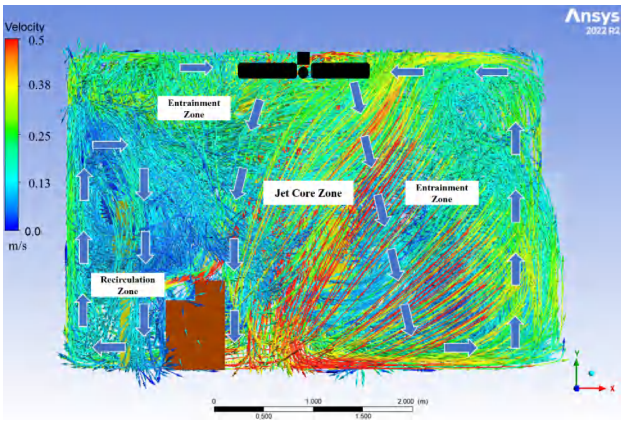

Figure 8. Velocity flow diagram of CF-1 (RPM120) under operation.

Wind speed was measured beneath CF-1 during its operation. During the measurement process, the anemometer sensor generated a small amount of heat, which could induce localized turbulence and thereby compromise the accuracy of the recorded data. To enhance measurement reliability, a turbulence kinetic energy (TKE) adjustment method was employed to correct the measured values. In this method, the corrected wind speed was calculated by integrating the measured three-dimensional velocity components (x, y, and z directions) with the turbulence kinetic energy (k) term [17]. The correction equation is

$$V = \sqrt{u^2 + v^2 + w^2 + f(k)} \quad (5)$$

where u, v, and w are the velocities (m/s) in direction x, y, and z, respectively. $f(k)$ denotes the adjustment factor of the turbulent kinetic energy to the wind speed to compensate for the effect of turbulence due to heat loss from the thermal sensor.

Figure 9 compares simulated and measured wind speeds for CF-1. Measurements were taken at heights of approximately 0, 0.5, 1.1, and 1.75 m. Overall, the simulation captured the measured trend at all locations. The measured speed at 1.1 m was higher than the simulated value, which may be due to the inclusion of a standing occupant in the CFD model and to the directional sensitivity of the thermal anemometer. The mean absolute percentage error (MAPE) was below 13.85% and the root mean square error (RMSE) was 17.18%, both within the ≤20% range commonly considered acceptable for indoor airflow validation. Although a small number of velocity data points do not match exactly, these discrepancies do not materially affect the airflow analysis in this study.

Figures 8 and 10a,b show the flow velocity streamlines for the CF-1, CF-3, and CF-6 respectively. Consistent with previous studies, the three operating modes exhibit a distinct downward jet core, as highlighted by Omrani, Matour [34]. The gradual reddening of the streamlines in the simulation results indicates that airflow velocity increases with fan speed, while the overall jet-core structure remains similar. Interestingly, regardless of CF speed, the streamline color shows that airflow velocity behind the cash register is consistently lower than in other parts

of the room, suggesting that the counter acts as a physical barrier. Whether this local sheltering benefits or hinders overall room mixing warrants further investigation.

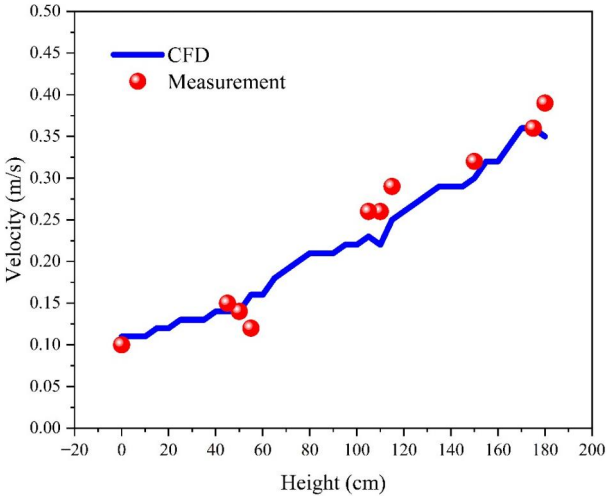

Figure 9. CF-1 flow field wind speed validation.

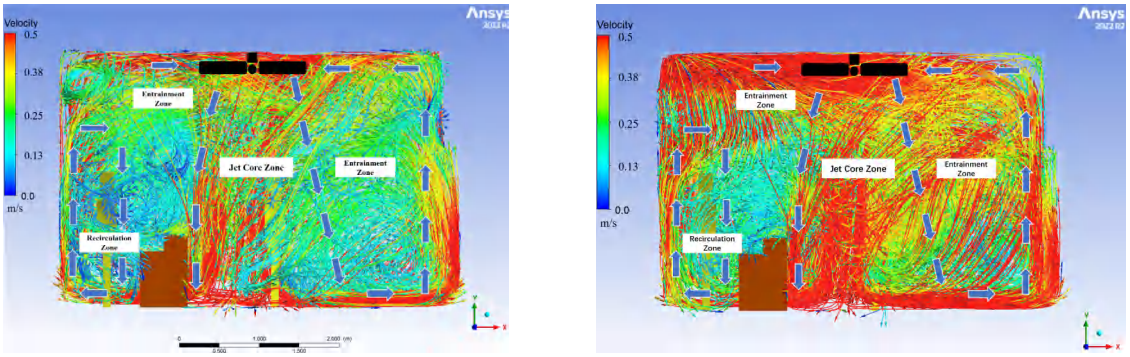

(**a**) (**b**)

Figure 10. Velocity flow diagram of (**a**) CF-3; and (**b**) CF-6 operation.

Figure 11 shows velocity contours through the fan center under CF-1, CF-3, and CF-6. The jet core forms the highest-velocity region and decays in a downward, trapezoidal pattern [34]. In all three cases, a near-floor high-velocity layer develops, with lower velocities under CF-1 and stronger coverage under CF-3 and CF-6; this layer is mainly distributed 0.2–0.4 m above the floor and thickens as fan speed increases. Figure 11b, further shows that only a small portion of the upper region is affected under CF-1, whereas under CF-3 the influence extends to the ceiling in the non-fan area. At CF-6, velocities in the upper region are markedly higher, indicating a stronger upward return flow.

A key operational parameter is fan rotation direction, which substantially alters the induced airflow field. Figure 12 illustrates the flow paths under upward-rotating operation, including UCF-1 (Figure 12a), UCF-3 (Figure 12b), and UCF-6 (Figure 12c). The upward jet impinges on the ceiling, spreads along it, descends near the walls, and then recirculates back towards the fan [34]. Unlike the downward-rotating mode, the flow generated by UCF is less influenced by the table, likely because it is distributed from above across the room.

The wind speeds were measured and recorded at room corners at heights of 1.1 and 1.7 m. As shown in Figure 13, the predicted velocities at almost all measurement points agreed with the measurements, with a MAPE below 11.5% and an RMSE of 16.3%.

From the cloud plot of the comparison between the velocities of the UCFs in Figure 14, there is no longer a distinct high velocity region in the room. The UCFs deliver airflow to the top of the room and form a high velocity layer near the ceiling, the thickness of which increases as the rotational speed gets larger. The appearance of a high velocity layer on all four walls is also observed in Figure 14a,b. The high-speed layer along the wall Figure 14c–f thicken with increasing rotational speed and extends further downward.

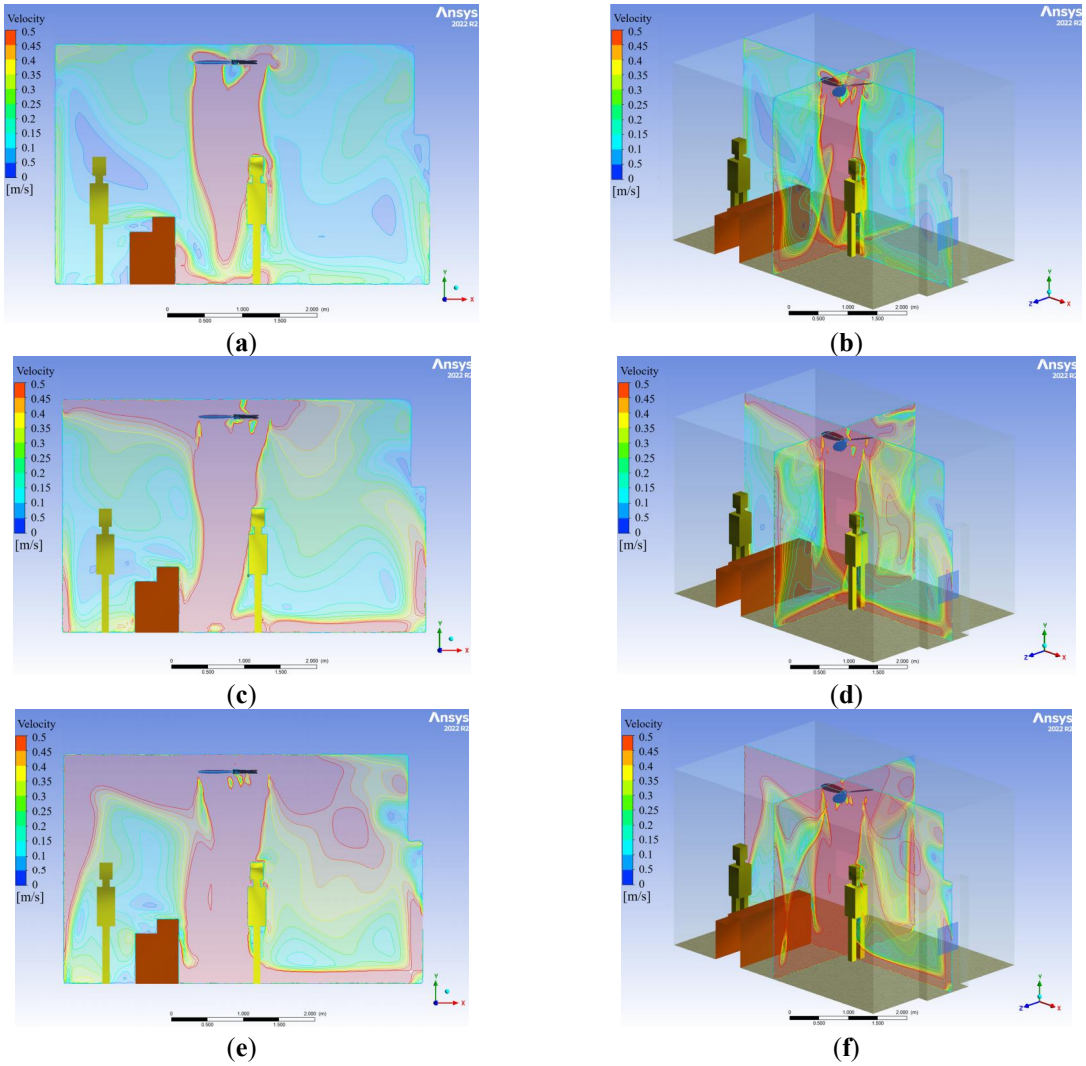

Figure 11. Velocity cloud of CF-1: (**a**) (z = 2.4), (**b**) (z = 2.4, x = 1.8); Velocity cloud of CF-3: (**c**) (z = 2.4), (**d**) (z = 2.4, x = 1.8); Velocity cloud of CF-6: (**e**) (z = 2.4), (**f**) (z = 2.4, x = 1.8).

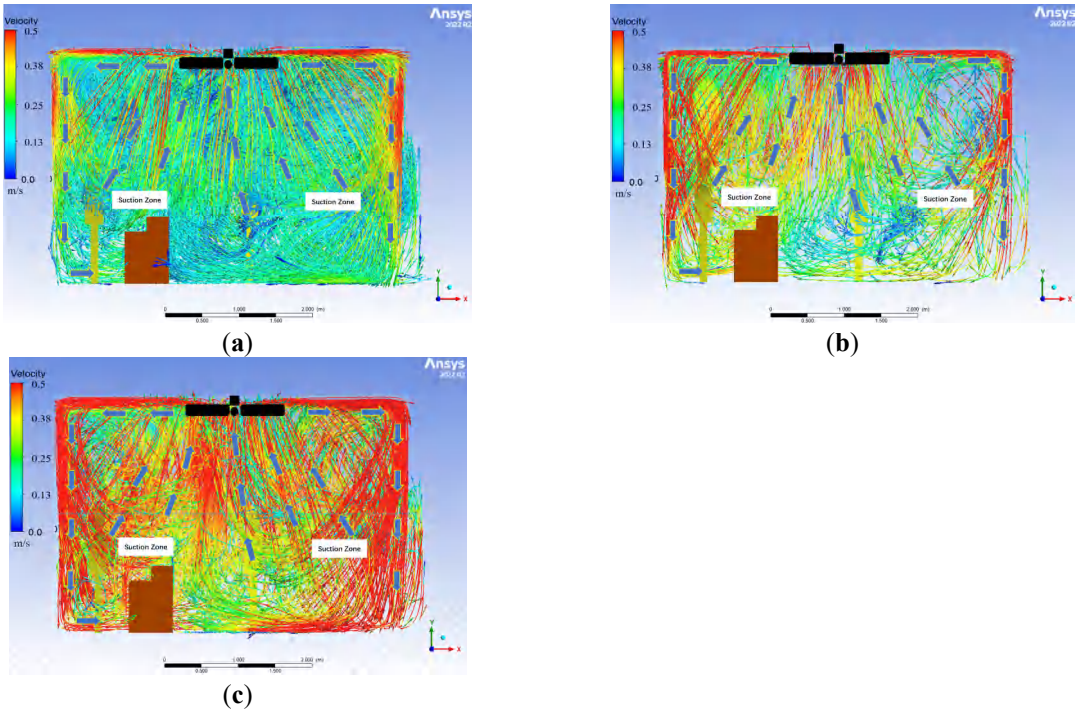

Figure 12. Velocity flow diagram of an upward rotating ceiling fan: (**a**) UCF-1; (**b**) UCF-3; (**c**) UCF-6.

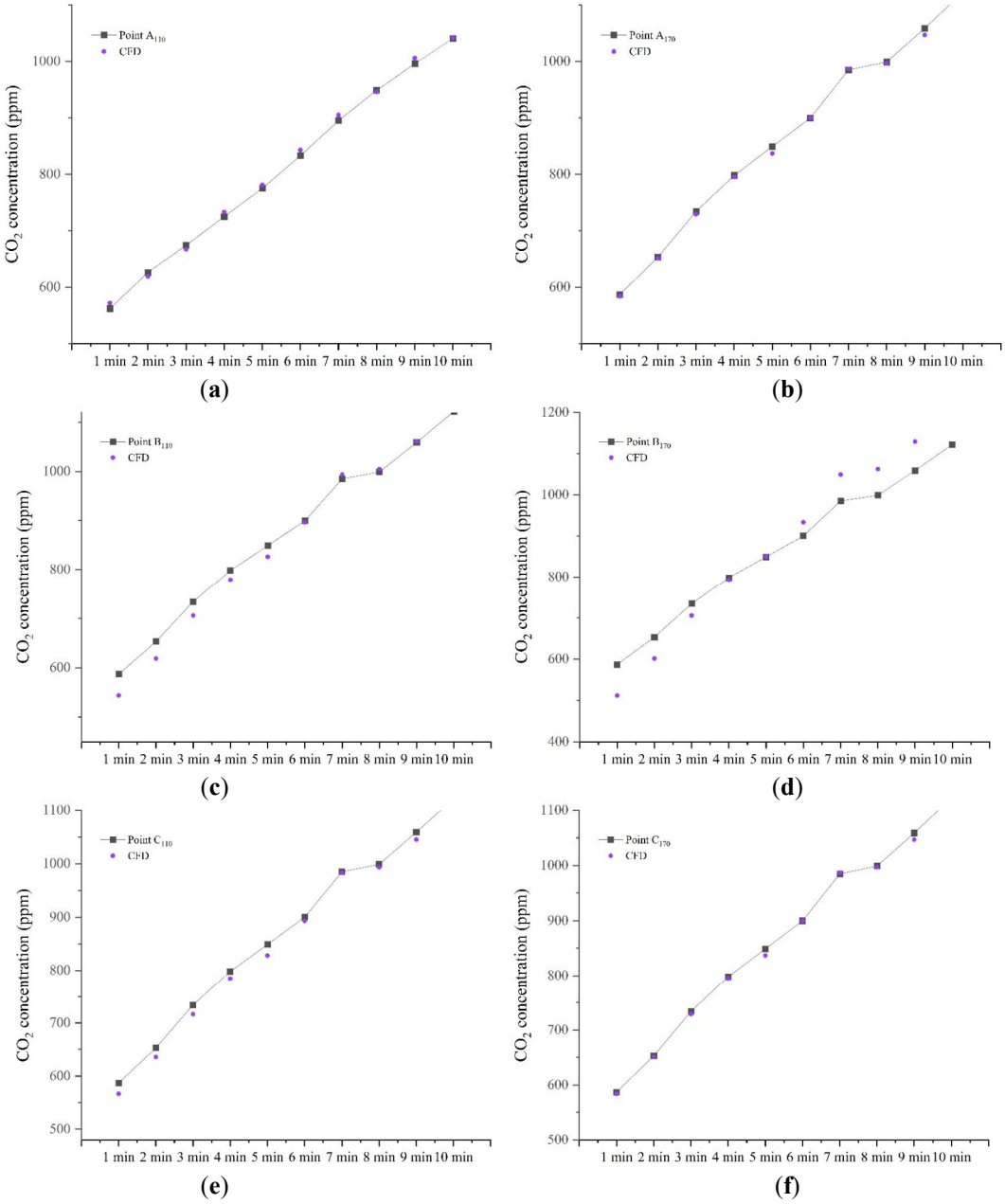

Figure 13. UCF-1 flow field wind speed validation: (**a**) point A110, (**b**) point A170, (**c**) point B110, (**d**) point B170, (**e**) point C110, (**f**) point C170.

At UCF-1, the flow rate below the CF is slightly higher than the other areas (as shown in Figure 14a,b). As the speed increases to UCF-3 and UCF-6, the CF influences airflow over a larger area. This effect likely occurs because, as the speed increases, a greater volume of airflow is drawn into the UCF from below. The $x = 1.8$ slices in Figure 14d,f reveal that the indoor flow field is divided into two layers: an upper and a lower layer. The lower layer (below 0.5 m) contains a slow vortex region, which may be caused by the presence of the cash register. Both CF and UCF flows are affected by checkout counters, which means that the role of checkout counters in street stores is worth investigating.

Experimental data from the tracer gas decay test was used to calculate the ACH in the street store under different fan influences, as shown in Table 7 The statistical results revealed that with CF-1 operation, the ACH in the room increased, with 3.28 in the center and 3.35 in the corners, higher than the average value of NV. The fan speed of CF-3 is 1.6 times that of CF-1, yet the ACH nearly doubles compared to CF-1 operation, indicating that the increase in fan speed significantly enhances indoor-outdoor air exchange. Under CF-6 operation, the ACH values at the center and corners of the room are 7.69 and 7.75, respectively. Compared to CF-1, CF-6 demonstrates a substantial improvement in ACH efficiency. For the upward rotation of CF, Table 8 indicates that the ACH values for UCF-3 and UCF-6 are 1.74 and 1.65 for UCF-3, and 2.83 and 2.93 for UCF-6, respectively. Clearly, the ACH values at both the center and corners are not favorable for indoor-outdoor air exchange. The measured

values for both are generally lower than NV (2.9), particularly for UCF-3, which may be attributed to UCF's influence on indoor airflow, causing a greater portion of airflow to participate in indoor recirculation rather than indoor-outdoor exchange.

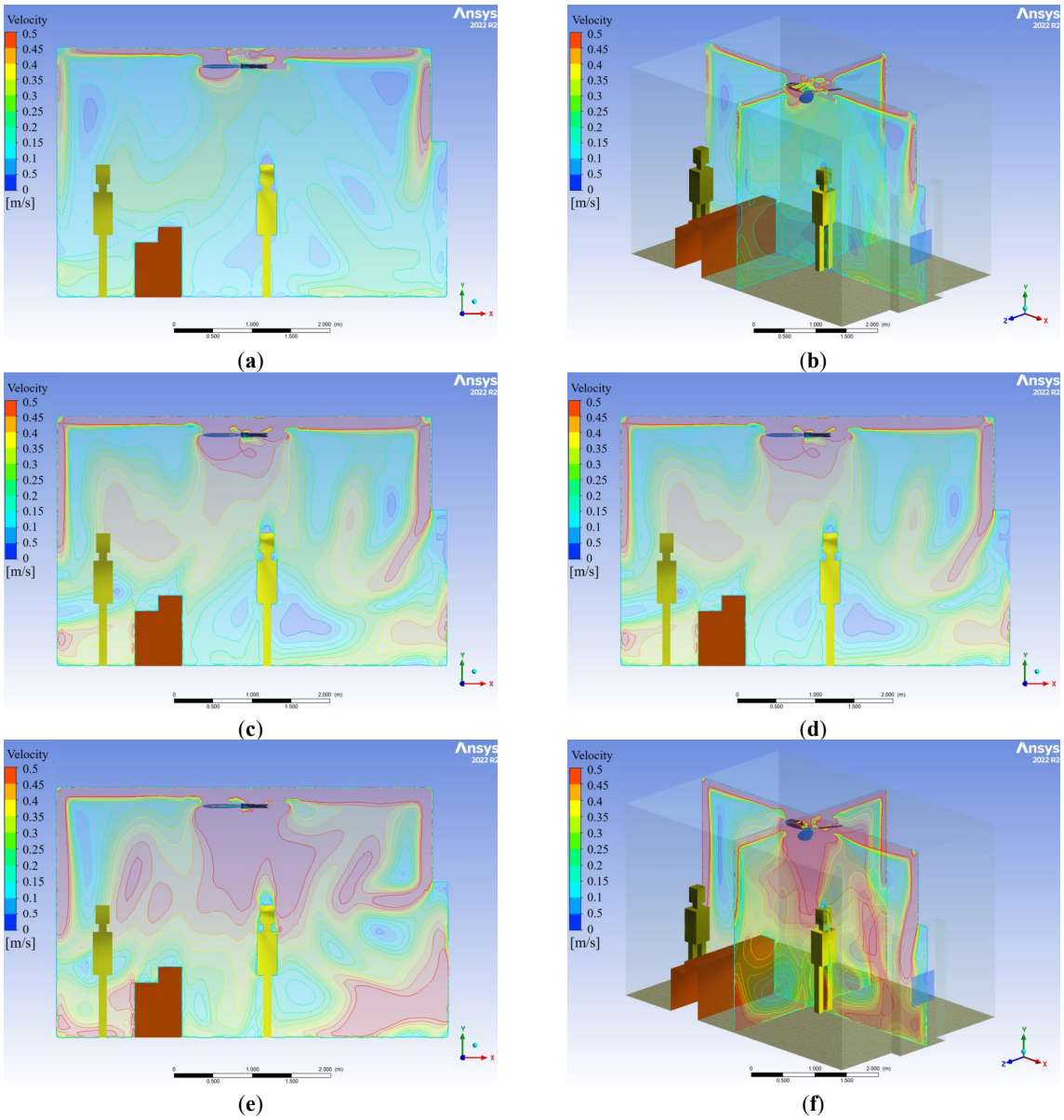

Figure 14. Velocity cloud of UCF-1: (**a**) (z = 2.4), (**b**) (z = 2.4, x = 1.8); Velocity cloud of UCF-3: (**c**) (z = 2.4), (**d**) (z = 2.4, x = 1.8); Velocity cloud of UCF-6: (**e**) (z = 2.4), (**f**) (z = 2.4, x = 1.8).

Table 7. ACH of fan ventilation.

Measurement Point	Height (cm)	Initial Concentration (ppm)	Final Concentration (ppm)	Time (min)	ACH
CF-1	Center	1157	670	10	3.28
	Corner	1228	703	10	3.35
CF-3	Center	2003	670	10	6.57
	Corner	2005	698	10	6.33
CF-6	Center	2402	666	10	7.69
	Corner	2351	646	10	7.75
UCF-3	Center	1257	941	10	1.74
	Corner	1250	950	10	1.65
UCF-6	Center	1373	856	10	2.83
	Corner	1447	888	10	2.93

Table 8. The relationship between the duration of guests' stays in the room and the probability of infection under different ventilation strategies.

	Time	CF-3	CF-6	NV+CF-3	UCF-3	NV+UCF-3	NV
Breathing zone	3 min	1.4%	1%	1%	1.4%	1%	7.6%
	10 min	11.3%	9.8%	6.9%	17.3%	10.4%	16.8%
Whole room	3 min	2%	1.3%	1%	2.3%	2.4%	3.8%
	10 min	11.7%	10.4%	4.7%	13.2%	9%	15.7%

3.2. Effect of Ceiling Fan Ventilation on Virus Transmission

The CF-induced airflow reshapes the tracer-gas distribution and, consequently, the estimated infection risk. Figure 15 presents the concentration evolution at point A (the breathing zone below the CF, 1.65 m above the floor) and point B (a non-fan area near the doorway, 1.65 m above the floor) over the 10-min test period. Figure 15a–c show results for CF-1, CF-3, and CF-6, respectively, and Figure 15d shows the natural-ventilation (NV) case. Overall, CF operation reduced breathing-zone concentrations by approximately 100–300 ppm over 10 min compared with NV. ANOVA indicated significantly higher concentration-reduction efficiency for each CF mode relative to NV (p = 0.007, 0.003, and 0.001 for CF-1, CF-3, and CF-6, respectively). Across all cases, concentrations at both points increased over time, reflecting continued mixing within the store. CF-6 yielded the slowest increase, remaining below 700 ppm at 3 min and approaching 1000 ppm at 10 min. CF-3 performed moderately well (below 700 ppm at 3 min) but exceeded 1000 ppm by 10 min. By contrast, NV and CF-1 performed poorly, reaching approximately 1200 ppm and 1000 ppm at 10 min and 3 min, respectively, which are above the acceptable range. A significant difference was observed between CF-3 and CF-1 (p = 0.02).

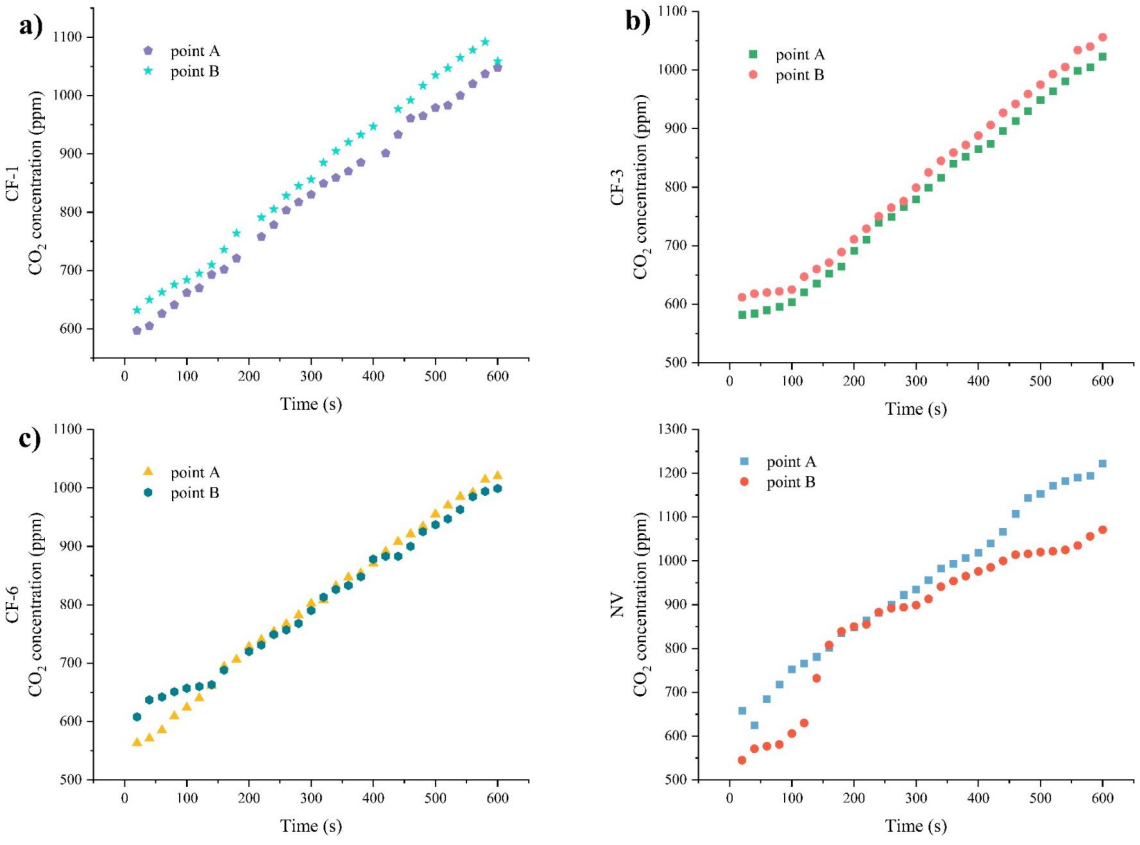

Figure 15. Concentration distribution at different ceiling fan speeds: (**a**) CF-1, (**b**) CF-3, (**c**) CF-6, and (**d**) NV.

Therefore, the relationship between height and concentration under CF-3 and CF-6 operations was examined in more detail. Figure 16a shows the CO_2 concentration values at three heights below the ceiling fan under CF-3. The results show that the CO_2 concentrations at both A110 and A50 are higher than at point A175. This may be because the fan continuously forces the released CO2 downward and promotes mixing. Similar behavior is observed for CF-6 (Figure 16b): the lowest concentration occurs in the breathing zone directly below the ceiling fan, whereas the highest concentration occurs at 110 cm. This may be disadvantageous in spaces occupied by both adults and children.

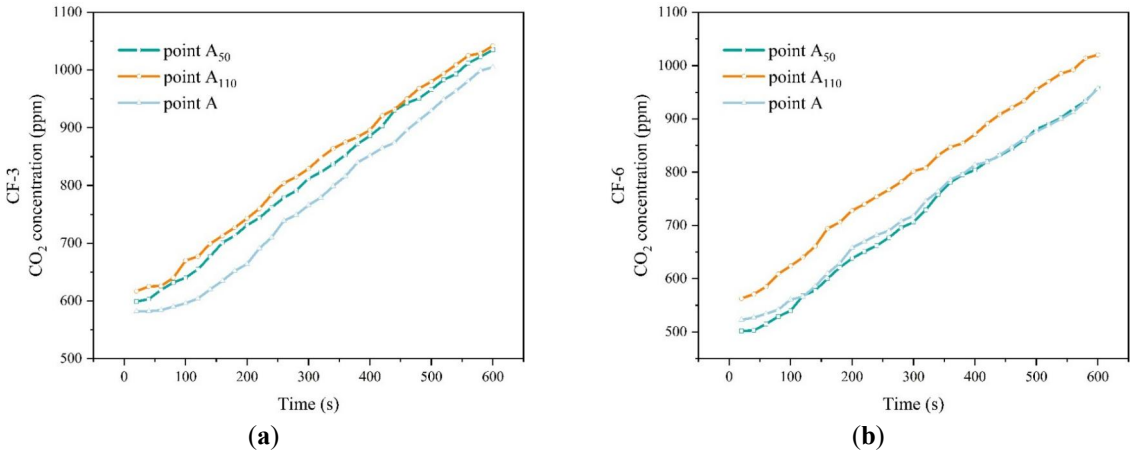

Figure 16. Concentration values at different heights below ceiling fans: (**a**) CF-3; (**b**) CF-6.

Because the release point is below the CF and adjacent to point A, concentrations at point B are consistently lower than at point A under NV Figure 15d. When the fan was operated, the lower breathing-zone concentration at point A was also observed for CF-1 and CF-3 (Figure 15a,b). Under CF-6, concentrations at points A and B were similar (Figure 15c). These measurements suggest that CF-3 and CF-6 suppress exhaled pollutants near point A within the first 3 min. Both CF-3 and CF-6 substantially reduced overall concentrations in the room, and the difference between them was not pronounced, implying limited benefit from increasing fan speed beyond CF-3. CF operation also influenced concentrations at point B, following a similar trend to the distribution directly below the fan.

Wells-Riley calculated the probability of infection at each measurement point for 3 min and 10 min in the street store. The probability of infection at 3 min for CF-3 and CF-6 personnel entering the store is well controlled, with the probability of infection in the center of the room at 3 min being 2% and 1.5%, respectively, and the probability of infection in the corners of the room being much lower than 10%, which meets the requirements for commercial buildings in general. However, the infection probability under both operations after 10 min becomes 11.3% and 9.8%, respectively. A probability of infection within 10% is also accepted, and the standard only applies to places where people stay for a short time. Thus, only CF-6 was still within the safe range after 10 min, but the probability of infection in the corner of the room under this operation was already undesirable at 11.2%, and the store was close to the critical value at this point.

In addition, the results of simulating particle diffusion for 0–3 min are shown in Figure 17. After the particle trajectories were visualized and the personnel started to spray the particles for 10 s, all the particles of CF-1 and CF-3 were pressed downward, but due to the fast air velocity of the CF operation of CF-6, a small portion of the particles had already diffused to the upper part of the room and to the "cashier's area". At 30 s, the particles under the operation of CF-1 and CF-3 had a similar diffusion pattern, and the particles in the "checkout area" were still relatively small. At 1 min, the measured results above show that the tracer gas is still within acceptable limits, but Figure 17c,h,m shows that the ejected particles have spread to most of the space inside the street store. Fortunately, there were relatively few particles in the checkout area, and the table hindered the spreading of particles. But at 3 min, it was not safe, although there were also relatively fewer particles in this area compared to other areas. However, most studies have emphasized the importance of prioritizing the reduction of concentrations in the breathing zone [35].

The simulation software counted the number of particles captured on customers and employees. The results of this study indicate that higher rotational speeds not only accelerate the diffusion of particles throughout the room but also significantly increase the number of particles captured by employees (susceptible individuals). In particular, CF-3 and CF-6 operation captured approximately 1.5 times more particles than CF-1. However, increasing the rotational speed from CF-3 to CF-6 did not result in an exponential increase in particle capture, yielding only a 10% additional capture rate. This may be because, regardless of the increase in fan speed, virus particles eventually establish a stable flow field within the indoor space of the street store, leading to a similar number of particles being captured by personnel. However, the rotational speed of CF-1 is relatively low, and the indoor airflow rate remains slow, leading to fewer particles being captured by personnel. In summary, operating CFs mix indoor air and, due to their strong downward airflow, have a mitigating and diluting effect on the concentration of viral particles in the indoor breathing zone for a short period. However, irrespective of CF speed, if the releaser remains in the room, the concentration of virus particles will continue to rise.

However, under both UCF-3 and UCF-6 operation, the trend of concentration changes in the breathing zone at point A (center of the room) and point B (corner) are shown in Figure 18. Over time, though, the concentration

at point A is higher than that at point B, either in UCF-6 or UCF-3 mode. However, both modes lead to an increasing trend in indoor CO_2 concentration. The higher concentrations despite the increased air velocity of the UCF-6 mode may have accelerated particle dispersion and increased the risk of infection, suggesting that increasing the airflow rate was not effective in improving concentration control in the presence of an upwardly rotating CF. Therefore, the UCF-6 model is not an optimal strategy. In contrast, the UCF-3 mode resulted in a slower rise in concentration in the breathing zone. concentrations did not exceed 700 ppm at 3 min or 1000 ppm at 10 min, making it suitable for short-term control. In addition, the Wells-Riley model was used to calculate the risk of infection in the room under CF-3 operation. At 3 min, the infection risk in the center, corners, and staff locations of the room were 1.7%, 2.1%, and 5.2% respectively indicating that particle dispersion can be effectively controlled in the short term. However, after 10 min the infection risk increased to 10.8%, 11.7%, and 18.7% further demonstrating the inadequacy of the UCF-3 model for long-term particle control. This finding corroborates the simulation results, particularly concerning the infection risk at the employee's location. The UCF causes virus particles to gradually accumulate at that location, making their removal more challenging.

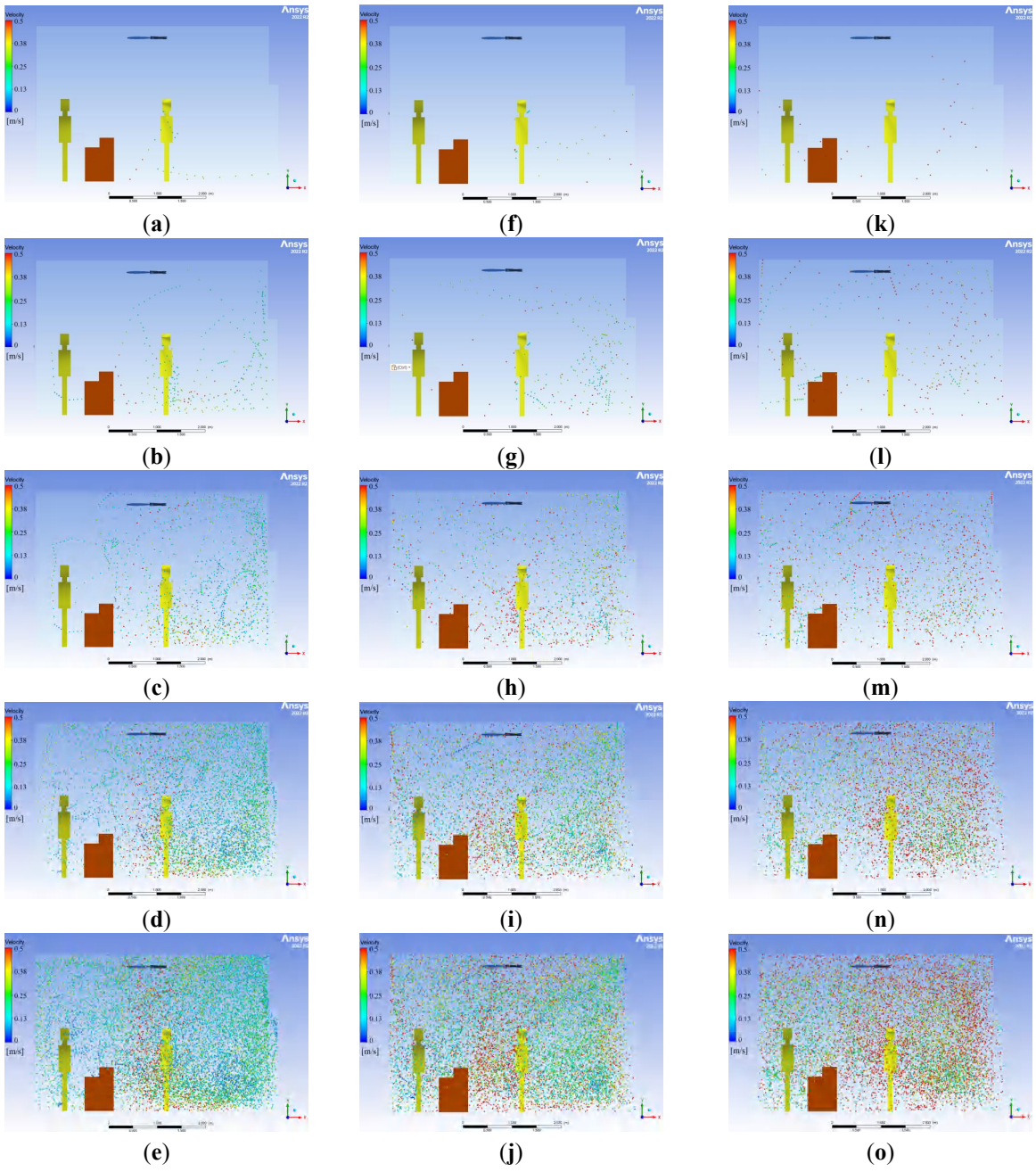

Figure 17. Particle distribution results at CF-1: (**a**) 10 s, (**b**) 30 s, (**c**) 60 s, (**d**) 120 s, and (**e**) 180 s; particle distribution results at CF-3: (**f**) 10 s, (**g**) 30 s, (**h**) 60 s, (**i**) 120 s, and (**j**) 180 s; and particle distribution results at CF-6: (**k**) 10 s, (**l**) 30 s, (**m**) 60 s, (**n**) 120 s, and (**o**) 180 s.

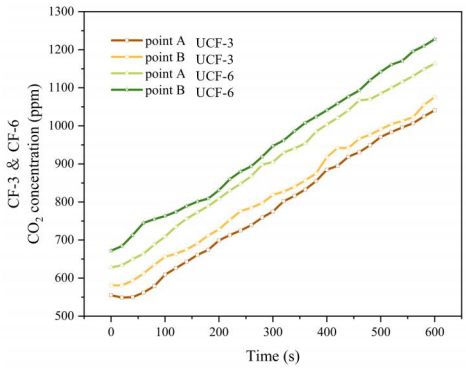

Figure 18. Concentration of UCF with time for different rotational speeds.

The result of the simulation, Figure 19, shows a room filled with particles for 60 s under UCF-3 operation. In fact, the simulation results revealed that while the risk of infection in the releaser's own breathing zone was not high, the employee location consistently had the highest risk of infection in the entire room. The particles were drawn upwards into the UCF-3 and redistributed in the room, and most of the distributed particles were dispersed downwards along the walls. Employees in close proximity to the walls are therefore at risk at this time. The particle captures statistics for employees indicate that the UCF-3 exhibits particle capture rates three orders of magnitude higher than those observed under CF operations.

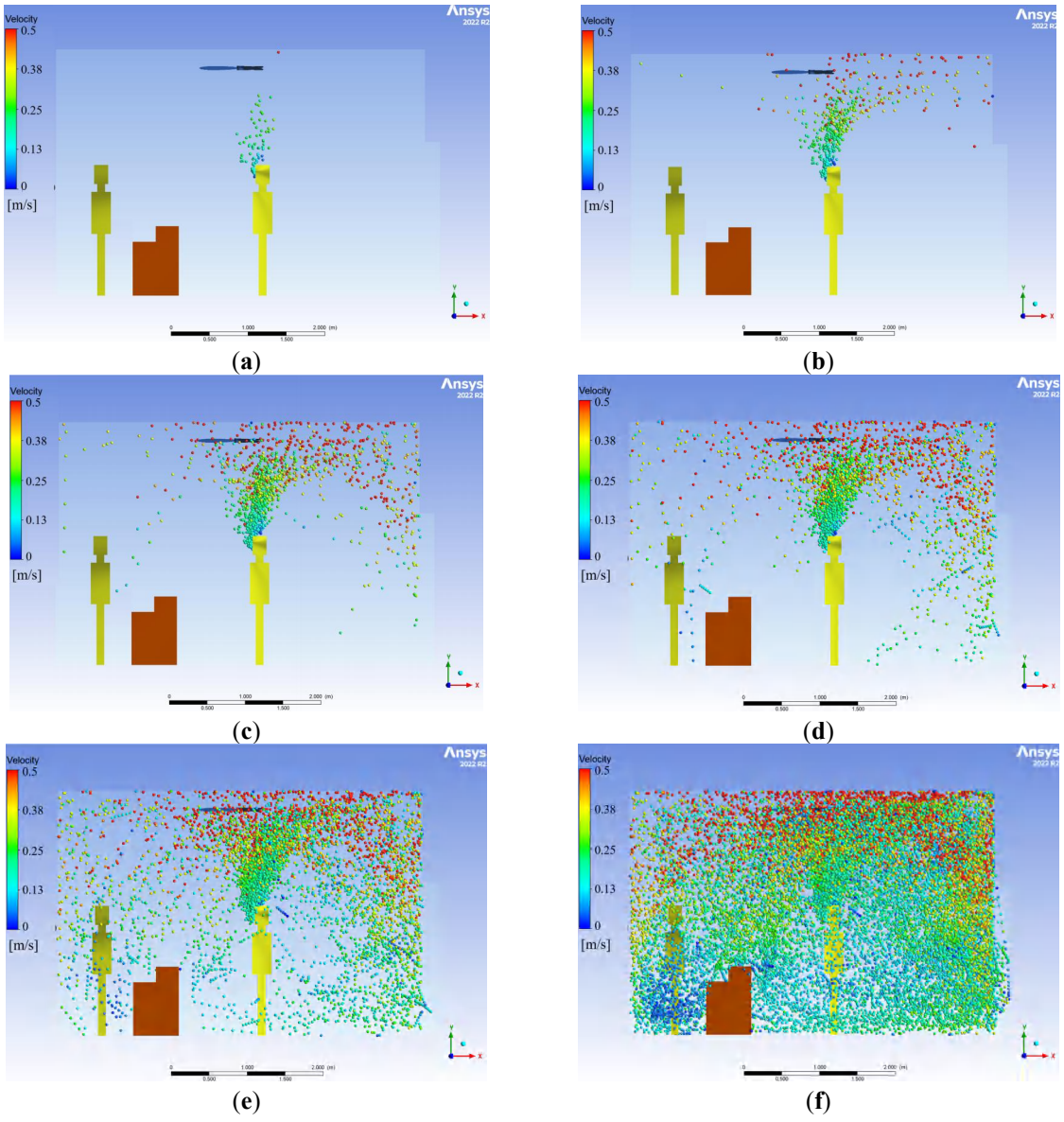

Figure 19. UCF-3 particle motion: (**a**) 5 s, (**b**) 10 s, (**c**) 15 s, (**d**) 20 s, (**e**) 30 s, and (**f**) 60s.

3.3. Effects of Combined Ceiling Fan and Natural Ventilation on Virus Transmission

Combinations of NVs and CFs are readily available as street stores may have their front doors open for long periods of time. When the CF was rotated downward, Figure 20a presents a comparison of the concentration at the breathing zone measurement point (Point A) under NV alone and in NV+CF. The results show that the concentration profile of the store under the NV alone is rising gradually and erratically, reaching approximately 1400 ppm after 10 min of testing at Point A. However, the other red line indicates the results of the NV+CF-3, where the concentration profile of the breathing zone under the CF over a 10-min period shows a horizontal profile, with an average concentration throughout of less than 600 ppm. The removal effect is highly significant, while the benefit of CFs in enhancing the store's ACH is also achieved.

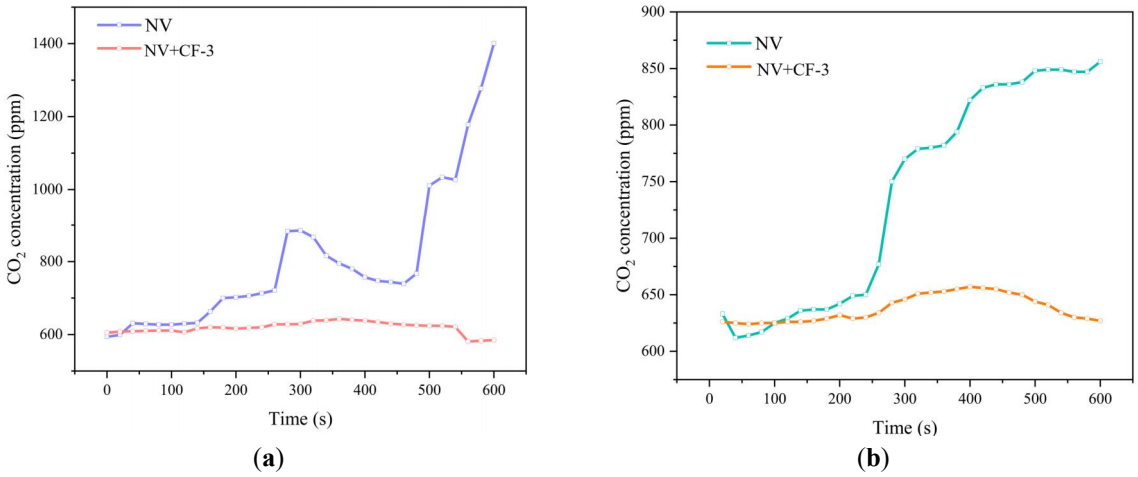

Figure 20. Comparison of different ventilation tracer concentrations: (**a**) point A; (**b**) point B.

In addition, under NV, the tracer gas concentration at the non-ceiling fan location (point B) was relatively low, being 550 ppm lower than that at point A after 10 min (Figure 20b). This indicates that concentration levels at different points in the room were unstable under NV conditions. Under the NV+CF-3 mode, the concentration at point B remained within the safe range of 600–650 ppm. The infection probability at point A was calculated as 1.9% at 3 min, while at the room corners it was 2.0%. After 10 min, the infection probability increased to 6.4% at point A and 6.9% at point B. On average, NV+CF-3 reduced the overall infection probability in the room by 4.5%. Therefore, NV+CF-3 hybrid ventilation represents an effective strategy and is particularly suitable for street stores where occupants spend extended periods of time.

In fact, it was originally predicted that NV+CF-6 would be the fastest fan ventilation strategy for expelling virus particles from a street store. As it turns out, the indoor airflow is too fast due to the high rotation speed, and the airflow pattern formed by the CF dominates the whole flow field, and some particles are carried away by the airflow back to the indoor flow field even before they can be discharged from the doorway. As a result, the indoor corner concentration of NV+CF-6 is higher. However, the flow field is diluted, which temporarily alleviates the virus concentration in the indoor breathing zone, but the risk of infection after 10 min is close to the critical value of 9.7%.

In addition, the NV+UCF as in Figure 21, the CO_2 concentrations at both points A and B increased during the test. For the breathing zone below the CF (green curves), both NV+UCF-3 and NV+UCF-6 operations were less than 700 ppm after 3 min and did not exceed 800 ppm after 10 min, which were both in the acceptable range of performance, and the probability of infection for Points A and B for both were 2.1% and 2.2% and 1.9% and 2.0%, respectively. For the breathing zone in the corner of the room (red curve), a comparison of the blue curve in Figure 20b and the red curve in Figure 21a shows that the final concentration of point B was approximately 850 ppm for both NV only and NV+UCF-3 operations, and the concentration was not reduced for 10 min, and the effect of the non-ceiling-fan zone was not significant.

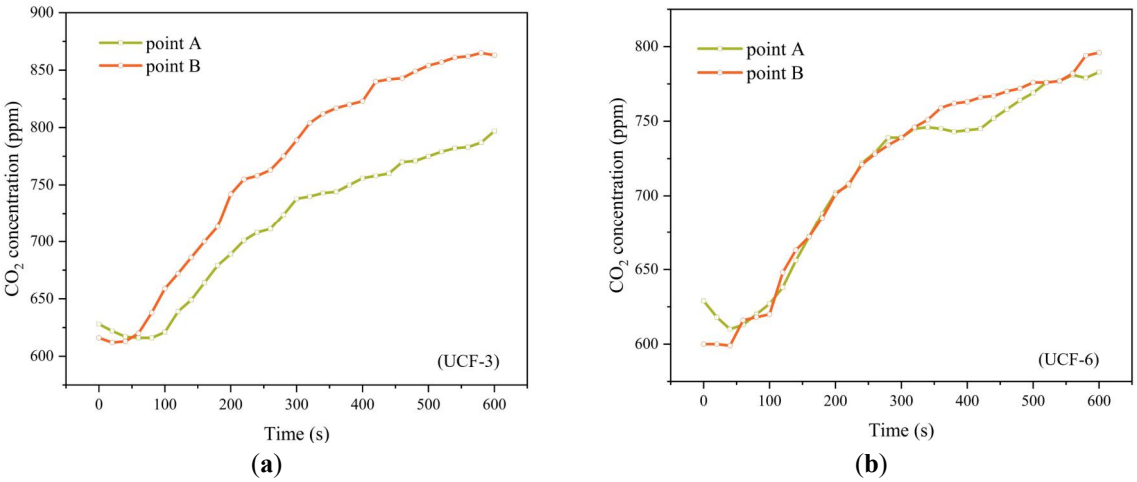

Figure 21. Concentrations measured at different speeds of the UCF: (**a**) NV+UCF-3; (**b**) NV+UCF-6.

This is due to the tracer released below the UCF being induced by the upward airflow and then participating in the circulating airflow from the UCF. The particles diffused from the ceiling close to the walls, which have aided the diffusion of the tracer gas. In addition, the probability of infection in the room with centers and corners under NV+UCF-3 and NV+UCF-6 operation was 9% and 10.4%, and 9.1% and 9.9%, respectively, within 10 min. Compared to using UCF alone, the fan mixing ventilation method reduces the concentration of particulate matter in the breathing zone below the CF within the room, thereby decreasing the probability of infection in the center of the room to an acceptable range. However, the risk of transmission in street stores remains, with the calculated infection risk value approaching the critical threshold. Additionally, the particle count analysis revealed that with increased natural ventilation, the number of particles captured by employees under UCF-3 operation decreased by 8%. In contrast, the number of particles captured by employees under CF-3 operation decreased by 48%. These findings indicate that NV+CF is a particularly effective ventilation strategy.

3.4. Impact of Time

This section will analyze the relationship between time and concentration. Since the relationship between time and infection risk is directly tied to practical exposure scenarios, all previously studied configurations were included in the infection probability calculations to ensure a comprehensive assessment across ventilation types.

Table 8 presents infection risks associated with 3- and 10-min exposures of Guest 2 under selected high-performance ventilation strategies, based on the tracer-gas experiment data in Section 3.2. All tested strategies except NV maintained infection probabilities below 2% in the breathing zone for a 3-min exposure, indicating relatively low transmission risk for brief visits following the departure of Guest 1 under effective fan-assisted ventilation. In such cases, infection prevention may focus on employee positioning and minimizing exposure to high-risk airflow zones. However, for a 10-min exposure, only NV+CF-3 kept infection probabilities below 10%. Although NV+UCF-3 also met this threshold, its less favorable dispersion pattern (as discussed above) may reduce robustness.

Efficient removal of residual contaminants is critical when Guest 1 leaves the store and Guest 2 enters shortly thereafter. To evaluate how well each strategy removes residual tracer, Table 9 summarizes the decay performance of residual CO_2 particles after the cessation of emission. The initial indoor concentration was set to approximately 2000 ppm, and reduction levels were assessed at 3 and 10 min across all strategies. The results show that CF-3, CF-6, UCF-3, and NV+UCF-3 performed poorly in the short term, with removal efficiencies below 20% after 3 min and remaining under 50% after 10 min. By contrast, NV+CF-3 achieved 53% removal at 3 min and 86% at 10 min, demonstrating clear effectiveness. NV+CF-6 further improved performance, reaching 70% and 98% removal at 3 and 10 min, respectively.

Table 9. Room removal efficiency with an initial concentration of 2000 ppm.

Time	CF-3	CF-6	NV+CF-3	NV+CF-6	UCF-3	UCF+NV
3 min	12%	11%	53%	70%	11%	17%
10 min	41%	44%	86%	98%	37%	47%

However, in practical applications, the initial indoor concentration may not reach 2000 ppm, as continuous implementation of ventilation strategies helps maintain lower background levels. Table 10 shows the CO_2 concentrations measured in the breathing zone during the first 10 min after the second visitor entered the room under different ventilation strategies. After 3 min, measurements under all fan strategies remained below 700 ppm; by 10 min, concentrations stabilized within the 600–1000 ppm range. These results indicate that continuous fan operation prevents excessive increases in indoor CO_2 levels. Consequently, the use of fan ventilation under actual environmental conditions significantly reduces infection risk.

Table 10. Breathing zone, indoor concentration of guests after entering for 1-10 min respectively (ppm).

Time	CF-3	CF-6	NV+CF-3	UCF-3	NV+UCF-3	NV
1 min	612	569	617	587	618	612
2 min	640	609	616	645	656	676
3 min	691	688	624	693	696	727
4 min	746	712	625	751	733	799
5 min	796	754	638	797	764	867
6 min	847	812	648	845	781	878
7 min	894	853	645	919	799	911
8 min	944	896	638	963	810	943
9 min	990	938	628	1005	822	992
10 min	1031	984	606	1059	830	1112

Based on Table 11 and the residual particle removal efficiency obtained from previous experiments, the time required for indoor concentrations to return to a safe level (600 ppm) was calculated under each ventilation strategy.

Table 11. The time required for the concentration to return to 600 ppm after Guest 1 leaves.

Guest1 departure time	CF-3 (min)	CF-6 (min)	NV+CF-3 (min)	UCF-3 (min)	NV+UCF-3 (min)
3 min	4.01	3.42	0.1	4.89	3.92
10 min	5.67	5.45	0.12	7.64	5.42

The results show that, under CF-3, CF-6, and NV+UCF-3 strategies, it takes approximately 6 min for the indoor concentration to decrease to 600 ppm after a 10-min stay by Guest 1, and about 4 min following a 3-min stay. Among these strategies, UCF-3 exhibited the slowest removal performance, requiring up to 30% more time to achieve concentration recovery compared to the others prior to the point of intersection.

After 10 min, only the NV+CF-3 strategy maintained CO_2 concentrations below 650 ppm. Under these conditions, the indoor environment is close to equilibrium, and particle concentrations can return to the safe threshold of 600 ppm within approximately 1 min after personnel leave, requiring minimal additional clearance time. NV+CF-3 consistently maintains low infection risk with reasonable clearance times, making it well-suited for continuous operation in typical street store environments.

4. Discussion and Limitation

The results indicate that when a store is closed and relies solely on a CF, fan speed strongly affects the dilution of airborne contaminants and the associated infection risk. Both CF-3 and CF-6 reduced the average breathing-zone concentration to below 700 ppm within 3 min and further lowered concentrations by 100–300 ppm over 10 min. Consistent with previous findings [18], higher fan speed accelerates dilution and dispersion; however, excessive speed may promote long-range transport into areas that would otherwise remain relatively safe. A previous study reported that a lower rotational speed (160 RPM) can achieve the highest particle deposition rate in residential environments, thereby reducing infection risk. Similarly, in the present study CF-3 (196 RPM) provided the most balanced performance, achieving effective dilution while limiting unnecessary spread. In practical terms, if fan speed is too low, airflow coverage and dilution are insufficient; if it is too high, dispersion throughout the store is accelerated, potentially increasing exposure of susceptible occupants (e.g., employees).

This phenomenon can be attributed to the turbulent airflow patterns generated by CFs: at higher speeds, they enhance particle mixing and diffusion, enabling rapid spread throughout the room and raising the likelihood of particle accumulation in sensitive zones, such as employee work areas. Furthermore, in residential buildings, where occupant flow is low and dwell times are relatively long, short-term particle control strategies are clearly unsuitable.

Specifically, the results of this study found that the concentration was highest at a height of 110 cm directly below the CF, which means that the CF will cause the trajectory of the ejected particles to shift downwards,

consistent with the study by Li [35]. However, this also reveals the limitation of CFs in suppressing particle diffusion, that is, their suppression effect on particle diffusion is not comprehensive. The height at which people sit and the height of the breathing zone for smaller minors indicate that CFs may exacerbate particle accumulation in specific areas, posing additional challenges to the infection risk of specific populations. Therefore, the downward airflow generated by the CF forms a horizontal diffusion upon contact with the ground, accompanied by turbulent backflow. This phenomenon has a better dilution effect on respiratory zone particles in fixed sitting environments (such as classrooms, offices), but in dynamic environments (street stores), particle accumulation may occur due to airflow interference. To optimize the particle distribution in street stores, further adjustments need to be made based on the activity height and airflow patterns of different groups of people.

After combining NV, the ventilation efficiency is significantly improved. The ventilation rate (3.28–7.75 ACH) in NV+CF mode is highly consistent with the ventilation rate (4.2–7.5 ACH) that the DOAS-CF system proposed by [17] performs well in the laboratory. The study by [17] used a combination of CFs and mechanical ventilation to provide fresh air indoors, effectively reducing concentration while improving airflow distribution. In contrast, this study used a combination of CFs and natural ventilation, and the advantage of this combination strategy lies in the synergistic effect of natural ventilation and CFs: natural ventilation introduces fresh air and provides outlets for particles, while CFs improve dilution efficiency by enhancing airflow distribution. However, the effectiveness of natural ventilation is easily affected by external environmental conditions such as wind speed, temperature difference, opening size and position, and its dilution efficiency may be affected by airflow instability. However, the combination of natural ventilation and CFs provides a low-cost feasible solution for resource limited street stores.

This study primarily considered the outdoor environmental parameters under relatively favorable conditions. However, in practice, the outdoor environment is highly dynamic and subject to considerable variability, including wind speed and direction, temperatures, and precipitation. Future research should simultaneously incorporate a more comprehensive and dynamic set of both indoor and outdoor environmental parameters.

5. Conclusions

This study investigated ventilation strategies in street stores, which are characterized by high pedestrian density and increased vulnerability during epidemics. Tracer gas experiments combined with CFD simulations were employed to assess how CF rotation direction, speed, and ventilation conditions influence indoor airflow characteristics and infection risk. Results showed that in enclosed environments, downward-rotating CFs effectively displaced viral aerosols away from the breathing zone. In contrast, UCFs drove airflow along enclosure surfaces, causing wider dispersion and eventual recirculation into the breathing zone, thereby offering limited benefit for reducing viral transmission. By comparison, opening the exterior door substantially enhanced particle removal efficiency—by approximately 60%—independent of the fan operation mode. With respect to fan speed, a moderate rotation setting (NV+CF-3) proved effective in expelling viral particles from the breathing zone. At low speeds, viral particles in the breathing zone remained insufficiently removed, while excessively high speeds, although reducing local concentrations more rapidly, promoted wider dispersion throughout the room.

Author Contributions

X.H.: writing—original draft preparation, conceptualization, methodology, and investigation. M.Q.: writing—review and editing, methodology, and funding acquisition. J.L., N.M., X.Y., and H.Z.: writing—review and editing, data curation, conceptualization. All authors have read and agreed to the published version of the manuscript.

Funding

This work was supported by the Talent Introduction Program of Xihua University (Grant No. ZX20250024).

Institutional Review Board Statement

Not applicable.

Informed Consent Statement

Not applicable.

Data Availability Statement

Not applicable.

Conflicts of Interest

The authors declare that they have no known competing financial interests or personal relationships that could have appeared to influence the work reported in this paper. Given the role as an Editorial Board Member, Haoxiang Zhan had no involvement in the peer review of this paper and had no access to information regarding its peer-review process. Full responsibility for the editorial process of this paper was delegated to another editor of the journal. Mingyuan Qin had involvement in writing—review and editing, methodology, and funding acquisition. The author(s) take full responsibility for the content of the published article.

Use of AI and AI-Assisted Technologies

No AI tools were utilized for this paper.

References

1. Corbett, E.L.; Watt, C.J.; Walker, N.; et al. The Growing Burden of Tuberculosis: Global Trends and Interactions with the HIV Epidemic. *Arch. Intern. Med.* **2003**, *163*, 1009–1021. https://doi.org/10.1001/archinte.163.9.1009.
2. Kolinski, J.M.; Schneider, T.M. Superspreading events suggest aerosol transmission of SARS-CoV-2 by accumulation in enclosed spaces. *Phys. Rev. E* **2021**, *103*, 033109. https://doi.org/10.1103/PhysRevE.103.033109.
3. Qian, H.; Miao, T.; Liu, L.; et al. Indoor transmission of SARS-CoV-2. *Indoor Air* **2021**, *31*, 639–645.
4. Li, Y.; Qian, H.; Hang, J.; et al. Probable airborne transmission of SARS-CoV-2 in a poorly ventilated restaurant. *Build. Environ.* **2021**, *196*, 107788. https://doi.org/10.1016/j.buildenv.2021.107788.
5. Wang, Z.; Jia, F.; Galea, E.R.; et al. Transmission of SARS-CoV-2 via larger respiratory droplets in a restaurant environment. *Saf. Sci.* **2025**, *191*, 106938. https://doi.org/10.1016/j.ssci.2025.106938.
6. Mihara, K.; Sekhar, C.; Takemasa, Y.; et al. Thermal comfort and energy performance of a dedicated outdoor air system with ceiling fans in hot and humid climate. *Energy Build.* **2019**, *203*, 109448.
7. Mat, M.N.H.; Basir, M.F.M.; Yusup, E.M. Fans deactivation for minimisation of airborne pathogen transmission: During Malaysians congregational prayer gathering in mosque. *Int. Commun. Heat Mass Transf.* **2021**, *129*, 105694. https://doi.org/10.1016/j.icheatmasstransfer.2021.105694.
8. Wei, L.; Liu, G.; Liu, W.; et al. Airborne infection risk in classrooms based on environment and occupant behavior measurement under COVID-19 epidemic. *Build. Res. Inf.* **2023**, *51*, 701–716. https://doi.org/10.1080/09613218.2023.2185584.
9. Somsen, G.A.; van Rijn, C.; Kooij, S.; et al. Small droplet aerosols in poorly ventilated spaces and SARS-CoV-2 transmission. *Lancet Respir. Med.* **2020**, *8*, 658–659.
10. Escombe, A.R.; Oeser, C.C.; Gilman, R.H.; et al. Natural ventilation for the prevention of airborne contagion. *PLoS Med.* **2007**, *4*, e68.
11. Robinson, M.; Stilianakis, N.I.; Drossinos, Y. Spatial dynamics of airborne infectious diseases. *J. Theor. Biol.* **2012**, *297*, 116–126.
12. Qian, H.; Zheng, X. Ventilation control for airborne transmission of human exhaled bio-aerosols in buildings. *J. Thorac. Dis.* **2018**, *10*, S2295.
13. Han, X.; Mahyuddin, N.; Qin, M.; et al. Effect of Different Mechanical Fans on Virus Particle Transport: A Review. *Buildings* **2025**, *15*, 303.
14. Schiavon, S.; Yang, B.; Donner, Y.; et al. Thermal comfort, perceived air quality, and cognitive performance when personally controlled air movement is used by tropically acclimatized persons. *Indoor Air* **2017**, *27*, 690–702. https://doi.org/10.1111/ina.12352.
15. Li, J.; Zuraimi, S.; Schiavon, S. Should we use ceiling fans indoors to reduce the risk of transmission of infectious aerosols? *Indoor Environ.* **2024**, *1*, 100039. https://doi.org/10.1016/j.indenv.2024.100039.
16. Sadripour, S.; Mollamahdi, M.; Sheikhzadeh, G.A.; et al. Providing thermal comfort and saving energy inside the buildings using a ceiling fan in heating systems. *J. Braz. Soc. Mech. Sci. Eng.* **2017**, *39*, 4219–4230. https://doi.org/10.1007/s40430-017-0859-9.
17. Li, W.; Chong, A.; Hasama, T.; et al. Effects of ceiling fans on airborne transmission in an air-conditioned space. *Build. Environ.* **2021**, *198*, 107887. https://doi.org/10.1016/j.buildenv.2021.107887.
18. Pandey, B.; Saha, S.K.; Banerjee, R. Effect of ceiling fan in mitigating exposure to airborne pathogens and COVID-19. *Indoor Built Environ.* **2023**, *32*, 1973–1999. https://doi.org/10.1177/1420326X231154011.
19. Yang, S.; Wang, L.; Raftery, P.; et al. Comparing airborne infectious aerosol exposures in sparsely occupied large spaces utilizing large-diameter ceiling fans. *Build. Environ.* **2023**, *231*, 110022. https://doi.org/10.1016/j.buildenv.2023.110022.
20. Wang, H.; Luo, M.; Wang, G.; et al. Airflow pattern induced by ceiling fan under different rotation speeds and blowing directions. *Indoor Built Environ.* **2019**, *29*, 1425–1440. https://doi.org/10.1177/1420326X19890054.

21. Pichurov, G.; Srebric, J.; Zhu, S.; et al. A validated numerical investigation of the ceiling fan's role in the upper-room UVGI efficacy. *Build. Environ.* **2015**, *86*, 109–119. https://doi.org/10.1016/j.buildenv.2014.12.021.
22. Zhu, S.; Srebric, J.; Rudnick, S.N.; et al. Numerical Modeling of Indoor Environment with a Ceiling Fan and an Upper-Room Ultraviolet Germicidal Irradiation System. *Build. Environ.* **2014**, *72*, 116–124. https://doi.org/10.1016/j.buildenv.2013.10.019.
23. Cui, S.; Cohen, M.; Stabat, P.; et al. CO2 tracer gas concentration decay method for measuring air change rate. *Build. Environ.* **2015**, *84*, 162–169. https://doi.org/10.1016/j.buildenv.2014.11.007.
24. Stadnytskyi, V.; Bax, C.E.; Bax, A.; et al. The airborne lifetime of small speech droplets and their potential importance in SARS-CoV-2 transmission. *Proc. Natl. Acad. Sci. USA* **2020**, *117*, 11875–11877. https://doi.org/10.1073/pnas.2006874117.
25. Qin, M.; Chew, B.T.; Yau, Y.H.; et al. A novel evaluation indicator and optimal heating strategy for using an intermittent-operation catalytic combustion heater in open cold environments. *Build. Environ.* **2024**, *252*, 111271. https://doi.org/10.1016/j.buildenv.2024.111271.
26. Qin, M.; Chew, B.T.; Yau, Y.H.; et al. Thermal comfort characteristics of a catalytic combustion heater under wind-chilled exposure. *J. Clean. Prod.* **2024**, *436*, 140701. https://doi.org/10.1016/j.jclepro.2024.140701.
27. Yang, L.; Ye, M. CFD simulation research on residential indoor air quality. *Sci. Total Environ.* **2014**, *472*, 1137–1144. https://doi.org/10.1016/j.scitotenv.2013.11.118.
28. Bahramian, A.; Mohammadi, M.; Ahmadi, G. Effect of indoor temperature on the velocity fields and airborne transmission of sneeze droplets: An experimental study and transient CFD modeling. *Sci. Total Environ.* **2023**, *858*, 159444. https://doi.org/10.1016/j.scitotenv.2022.159444.
29. He, Q.; Niu, J.; Gao, N.; et al. CFD study of exhaled droplet transmission between occupants under different ventilation strategies in a typical office room. *Build. Environ.* **2011**, *46*, 397–408. https://doi.org/10.1016/j.buildenv.2010.08.003.
30. Arjmandi, H.; Amini, R.; Fallahpour, M. Minimizing the respiratory pathogen transmission: Numerical study and multi-objective optimization of ventilation systems in a classroom. *Therm. Sci. Eng. Prog.* **2022**, *28*, 101052. https://doi.org/10.1016/j.tsep.2021.101052.
31. Huang, J.; Hao, T.; Liu, X.; et al. Airborne transmission of the Delta variant of SARS-CoV-2 in an auditorium. *Build. Environ.* **2022**, *219*, 109212.
32. Versteeg, H.K. *An Introduction to Computational Fluid Dynamics the Finite Volume Method*, 2nd ed.; Pearson Education: New Delhi, India, 2007.
33. Gao, N.; Niu, J.; Perino, M.; et al. The airborne transmission of infection between flats in high-rise residential buildings: Tracer gas simulation. *Build. Environ.* **2008**, *43*, 1805–1817. https://doi.org/10.1016/j.buildenv.2007.10.023.
34. Omrani, S.; Matour, S.; Bamdad, K.; et al. Ceiling fans as ventilation assisting devices in buildings: A critical review. *Build. Environ.* **2021**, *201*, 108010. https://doi.org/10.1016/j.buildenv.2021.108010.
35. Li, W.; Hasama, T.; Chong, A.; et al. Transient transmission of droplets and aerosols in a ventilation system with ceiling fans. *Build. Environ.* **2023**, *230*, 109988. https://doi.org/10.1016/j.buildenv.2023.109988.